Experimental and numerical study of a high-pressure waterjet

Oleg Urazmetov*[1], Marcel Cadet[2], Roman Teutsch[2], Christian Schindler[3], Sergiy Antonyuk[1]
[1]Institute of Particle Process Engineering, Technische Universität Kaiserslautern,
Gottlieb-Daimler-Str. 44, 67663 Kaiserslautern, Germany
[2]Institute for Mechanical and Automotive Design, Technische Universität Kaiserslautern,
Gottlieb-Daimler-Str. 42, 67663 Kaiserslautern, Germany
[3]Chair and Institute for Rail Vehicles and Transport Systems, RWTH Aachen University,
Seffenter Weg 8, 52074 Aachen, Germany
*Corresponding author: oleg.urazmetov@mv.uni-kl.de

Abstract
High-pressure waterjet (HPWJ) nozzles are used for cutting or for surface treatment such as cleaning, decoating and deburring. The flow within a HPWJ nozzle is compressible and turbulent due to the high water pressure and velocity. Depending on flow velocity and the geometry of the HPWJ nozzle a multiphase flow of liquid and vapor can occur. Outside of the nozzle, a highly complex turbulent waterjet breakup takes place. In order to increase the breakup length of the waterjet, geometric modifications inside the nozzle are required. On the other hand, wear resistance of a nozzle is highly desirable. In this study, the flow inside of a convergent waterjet nozzle was investigated by means of computational fluid dynamics. For the true geometrical model, µ-CT scans of the studied nozzle were used. A reverse engineering process provided the model of the nozzle. The diameter of the orifice was 0.5 mm and the inlet pressure was at 75 MPa. For the modeling of the multiphase flow, the Volume-of-Fluid (VOF) method was applied. Turbulence is also a major influential factor on the primary breakup and therefore the Large-Eddy-Simulation (LES) method was utilized. Since LES method requires good inlet boundary conditions for producing stochastic components of the velocity field, separate Reynolds-Averaged-Navier-Stokes (RANS) simulations for realistic inlet conditions were performed. The studied nozzle had a flow grid, which is located in front of the convergent part of the nozzle. The influence of the flow grid on the waterjet was investigated both in the simulation and in the experiment. To validate the simulations, the flow rates from the experiment were compared with the simulation. High-speed photography provided the spray angle of the waterjet. The results of this study showed that higher turbulence, which was produced by the cross-shaped flow grid, had a stabilizing influence on the primary breakup of the jet.

Keywords
high-pressure waterjet nozzle, CFD, VOF, spray, atomization, primary breakup, turbulence.

Introduction

High-pressure waterjet nozzles are widely used in a range of applications. Cutting with a pure HPWJ is limited to thin and soft materials. In order to cut thicker materials, abrasive particles are commonly mixed to form an abrasive waterjet [1]. For cleaning purposes, pure HPWJ is usually used [2]. In both cases, a high specific energy per unit area is desired. Therefore, almost all high-pressure nozzles work in the atomization regime as defined by [3]. Thus, under the present process conditions, atomization should occur directly at the nozzle outlet, which is not desired. It is known that the geometry of the nozzle has a significant influence on the waterjet breakup [4]. Many manufacturers design their nozzles in a special way to avoid a fuzzy jet. Experiments are often difficult due to the small dimensions of the nozzle, which hinders exact flow measurements, especially inside the nozzle. Stability analysis theories have been done in the past, but always neglected the flow field within the nozzle [5]. Therefore, numerical simulation of the flow inside the waterjet nozzle is often the only way to gain knowledge about the physical properties, such as turbulence values and velocity profiles. The aim of this study is to create a connection between the flow inside the nozzle and the influence on the atomization of the waterjet.

Theoretical velocity of the high-pressure waterjet flow

Since water becomes compressible at sufficiently high pressure, the error must be checked as to whether the water can be treated as incompressible or not. The following three equations are used to calculate the velocity of the jet with water as a compressible liquid [6]. With p as the pressure of water, the equation of state for density is:

$$\rho = \rho_0 \left(1 + \frac{p}{nK_0}\right)^n \qquad (1)$$

Where ρ is density with n as a density exponent and K_0 as the reference bulk modulus of water. Together with equation (1) and Bernoulli's equation for theoretical velocity v_{th} (2),

$$v_{th} = \sqrt{\frac{2p}{\rho}} \tag{2}$$

the jet velocity, v_j , can be found as [6].

$$v_j = \sqrt{\frac{2nK_0}{\rho_0(1-n)}\left[\left(1+\frac{p}{nK_0}\right)^{1-n}-1\right]} \tag{3}$$

At p = 75 MPa and a constant density of 998.2 kg/m³ equation (2) gives: v_{th} = 387.65 m/s. With compressible density and values for p = 75 MPa, n=7.15 and K_0 = 2.2 GPa (values for n and K_0 can be for example found in the online guide for Ansys Fluent [7].) the jet velocity becomes v_j = 384.34 m/s. The difference is small at 75 MPa but becomes more significant with higher pressure values.
Another important value for nozzle flow is the nozzle discharge coefficient c_d. By obtaining the volume flow, the discharge coefficient can easily be calculated using equation (4).

$$\dot{q} = c_d A_0 v_j \tag{4}$$

where A_0 is the area of the nozzle cross section.

Experimental setup

A plunger pump is generating the high-pressure water for the waterjet. The water flows through a hose from the pump to the nozzle lance. Inside the lance, there is a turbulent flow. Figure 1 shows the experimental setup. A Nikon d7200 CMOS camera with a Zeiss 50 mm, f/2 lens was used. Pictures were taken in a completely dark room with a relatively slow shutter speed of 1/15 s. Therefore, only the NANOLITE flash exposed the sensor. The aperture was set to f/2, which provided good light intensity and a sufficient good depth of field. To keep the spray development as low as possible, the water tank was covered with a plastic plate.

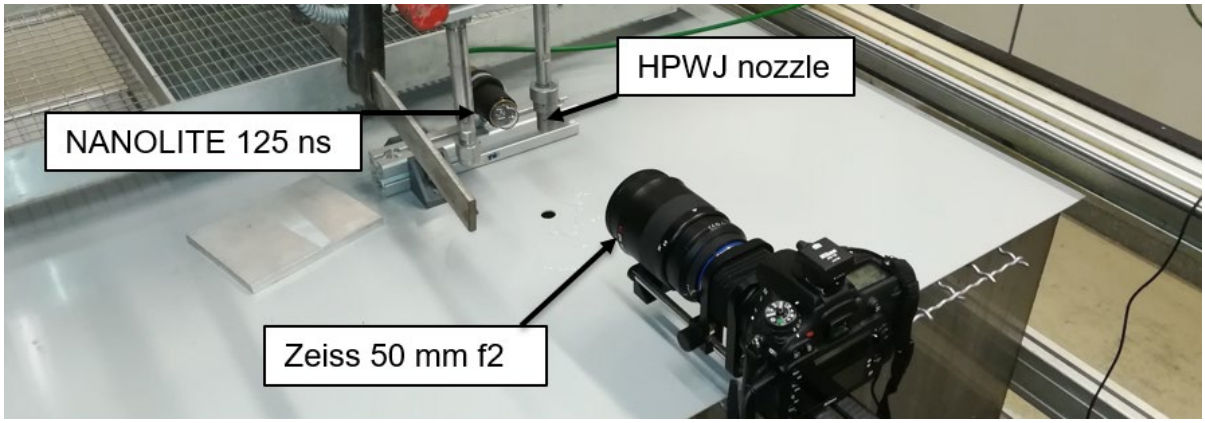

Figure 1. Experimental setup.

Simulation model

The simulation of the primary breakup is computationally very demanding, because of the high mesh density at the liquid/gas phase. Therefore, the simulation of the nozzle flow and the high-pressure waterjet were considered separately. Two simulation models had to be created. The flow inside the nozzle was numerically calculated from the nozzle lance to the nozzle outlet. The simulation of the high-pressure waterjet consists of a short cylindrical part (the total length of the nozzle was preserved) of the nozzle and a cylindrical surrounding area in which the jet breakup was calculated numerically. In order to design the nozzle geometry as realistically as possible, µ-CT scans were performed and the triangulated surfaces were reconstructed in a reverse engineering process, see Figure 2. The black box marks the area of interest of the water flow.

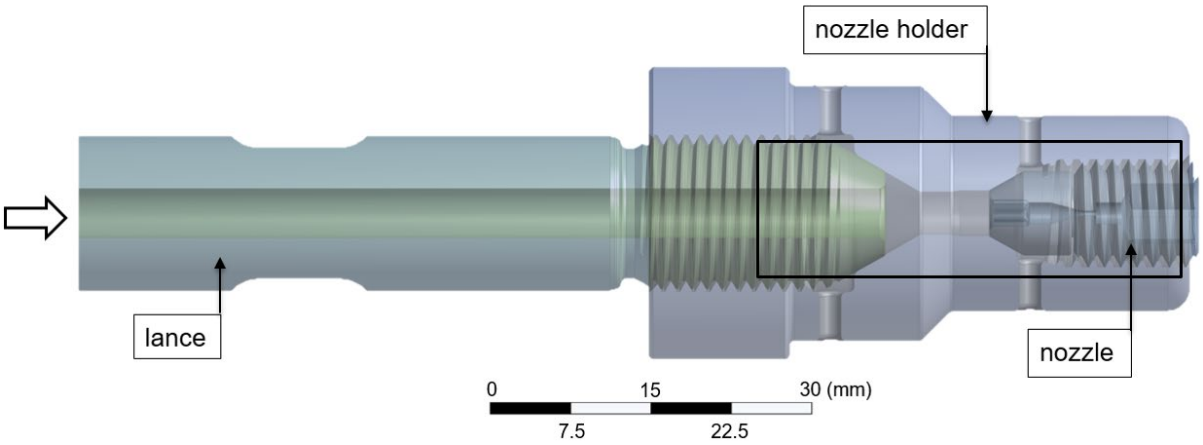

Figure 2. CAD assembly reconstructed from µ-CT scan (Arrow illustrates the direction of flow).

Although the nozzle was labeled as 0.5 mm in diameter, the generated model had 0.49 mm as the nozzle diameter. The reason for the deviation of both values could originate from the scan, however, the value is still in the tolerance of the nozzle. The specifics of the used nozzle are summarized in Table 1

Table 1. Geometry of the nozzle

	nozzle diameter	cone angle	l/d nozzle	nozzle edge radius
nozzle parameter	0.49 mm	30 degree	2.5	1 mm

Parameters of RANS and LES-VOF simulation

For the simulation of the flow inside the nozzle, a 3D interior volume was extracted from the location, which was marked by the black box in Figure 2. The extracted volume can be seen in Figure 3. The two colors in Figure 3 indicate the two simulation domains, grey for the RANS simulation and blue for the LES-VOF.

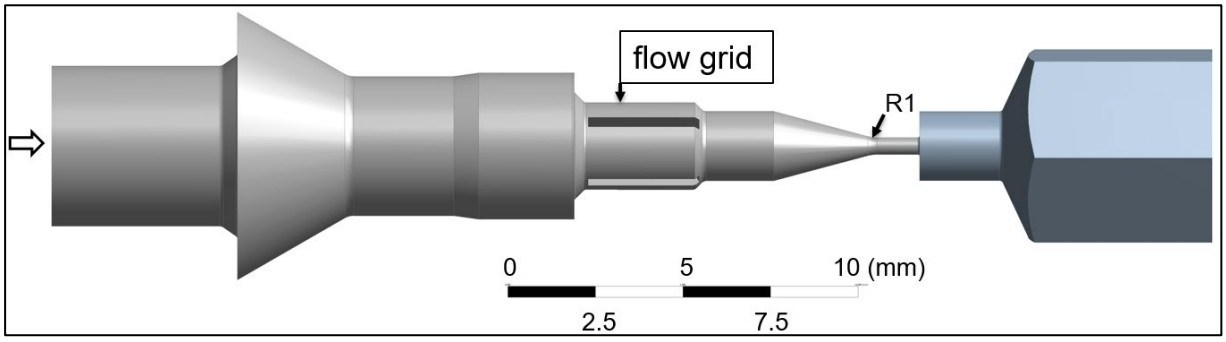

Figure 3. Extracted 3D interior volume (Grey volume: water under high pressure, blue area: air at ambient pressure).

For the RANS simulation, a hybrid mesh was generated with tetrahedral and hexahedron elements, Figure 4. The cylindrical part of the nozzle was meshed with hexahedron elements. For the more complex geometry, tetrahedral elements were used. From previous 2D simulations, the inlet edge of the nozzle was examined and no cavitation was detected with an inlet edge of 1 mm. Therefore, a single-phase simulation was set up. The modeling of the turbulence effects were carried out with the kω-SST model [8]. For the LES-VOF simulation, the geometry was reduced to the outlet part of the nozzle and a cylindrical volume in which the waterjet interacts with the quiescent air was added. The dimensions of the outflow space were simplified; the hexagonal socket was replaced with a cylinder. As for turbulence modeling the LES was used [9]. The results from RANS simulation were used as boundary conditions for the LES-VOF.

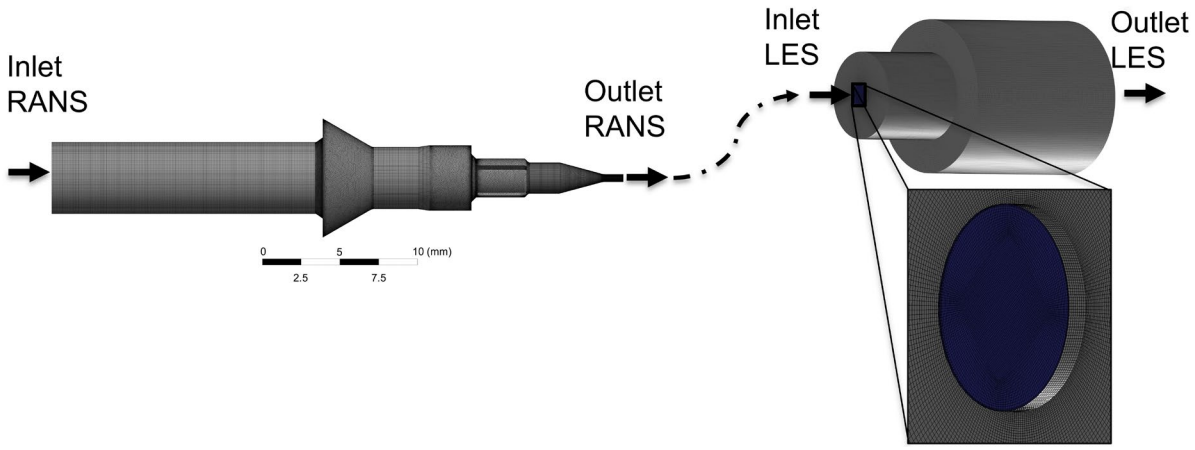

Figure 4. Mesh for the RANS simulation on the left side and mesh for the LES-VOF simulation on the right side (Arrow illustrates the direction of flow, walls are coloured in grey).

The properties of both the RANS and LES-VOF simulations are summarized in Table 2

Table 2. Mesh properties and simulation parameters

	RANS	LES-VOF
total cells	$2.9 \cdot 10^6$	$12 \cdot 10^6$
total length of the domain	37 mm	6 mm
total volume of the domain	$4.89 \cdot 10^{-7}$ m³	$4.43 \cdot 10^{-8}$ m³
turbulence model (y^+-value)	kω-SST (~35)	LES (~4.5)
boundary conditions	pressure inlet: 75 MPa pressure outlet: 0 MPa	velocity inlet: velocity. mag., tke and epsilon pressure outlet: 101325 Pa
fluid	water compressible	water/air incompressible
surface tension	-	$73.5 \cdot 10^{-3}$ N/m
Reynolds/Weber number	$2 \cdot 10^5$/-	$2 \cdot 10^5/1 \cdot 10^6$
time step	steady-state	14 ns (implicit)

RANS results

First, the results of the flow inside the nozzle are shown, Figure 5 and Figure 6 show the velocity field of the flow. For comparison reason, the flow grid was removed. Through the flow grid, there is a local speed increase. Additionally, the flow grid untwists the flow if there are some swirls present from the inlet boundary condition. However, the flow grid had no influence on the maximum velocity of the flow at the nozzle exit. In both cases, the maximum speed of around 385 m/s was reached, which is almost identical to the value calculated with equation (3). The volume flow rate was in both cases almost identical, around 4.15 l/min. The measurements of the flow rate with an ultrasonic flow meter fluctuated between 3.67 and 4.33 l/min, while the product data sheet of the manufacturer indicated the flow under the given conditions with 4.2 l/min. The simulation predicts the experimentally determined values for the volume flows. With the values for speed and volume flow rate, the discharge coefficient of $c_d \approx 0.96$ was determined. Table 3 illustrates the results of the influence of the flow grid. The discharge coefficient with the flow grid is slightly lower when compared to the nozzle without the flow grid. The reason is that the flow grid acts as flow resistance. However, the influence is negligibly small, due to the relatively low flow velocity. When comparing the nozzles with and without the flow grid, it becomes clear that the walls of the flow grid create turbulence in the flow core as indicated in Figure 7. The results of the RANS simulations are summarized in Table 3.

Table 3. RANS Results

	nozzle with flow grid	nozzle without flow grid
mass flow / kg/s	0.0691764	0.0692236
max. velocity / m/s	384.769	384.762
discharge coefficient / -	0.95619	0.95684
max. tke (nozzle outlet) / J/kg	1229	1070.6

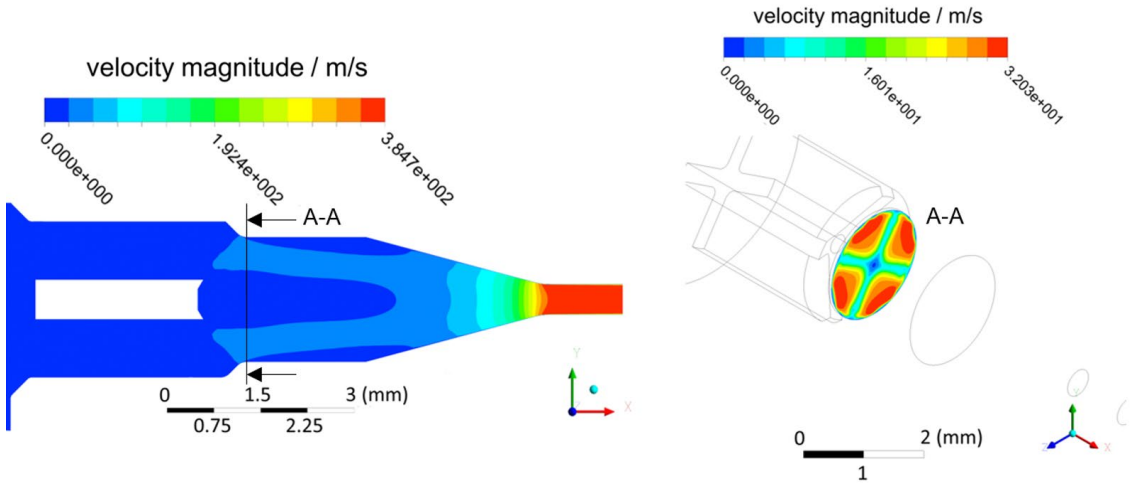

Figure 5. Velocity magnitude inside the nozzle with the flow grid.

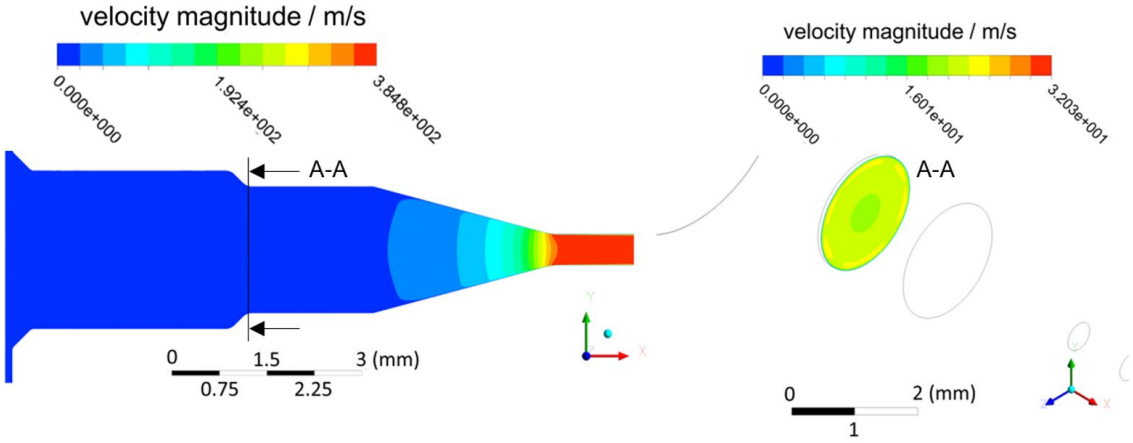

Figure 6. Velocity magnitude inside the nozzle without the flow grid.

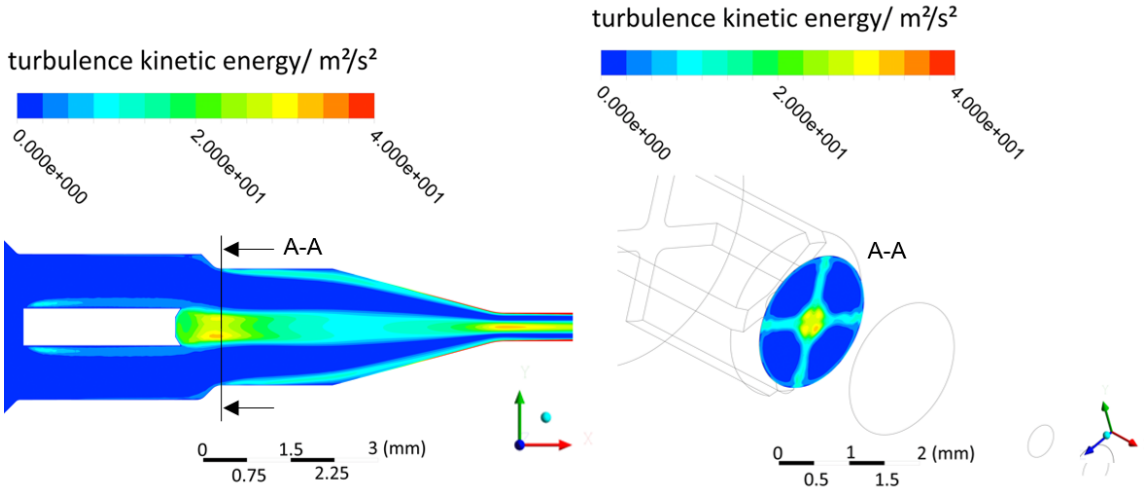

Figure 7. Contour plots of turbulence kinetic energy (tke).

As next, Figure 8 shows the velocity magnitude and the turbulence kinetic energy on the nozzle outlet for the nozzle with and without the flow grid. It is noticeable that the turbulence, produced by the flow grid, persists to the nozzle outlet. In addition, the absolute values for turbulence kinetic energy (tke), close to the wall, are up to 20% higher for the nozzle with the flow grid. The velocity field was found to be more irregular in the near wall region for the nozzle with the flow grid.

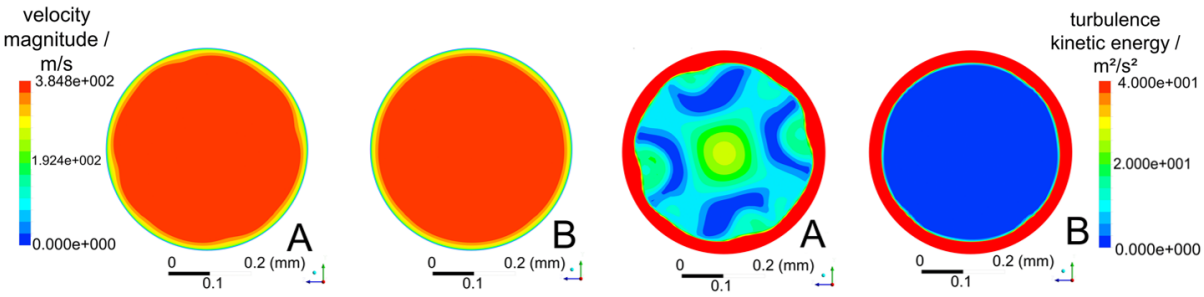

Figure 8. Contour plot of velocity magnitude (left side A and B) and turbulence kinetic energy (right side A and B), red areas are greater than/equal 40 m²/s², at the nozzle outlet (Nozzle type A: flow grid, nozzle type B: no flow grid).

LES-VOF results

As mentioned before, the data from the RANS simulation was used for the LES-VOF simulation as a boundary condition. To produce stochastic components from steady-state RANS simulation, the spectral synthesizer method was utilized [10]. The results of the LES-VOF simulations are summarized in **Table** 4.

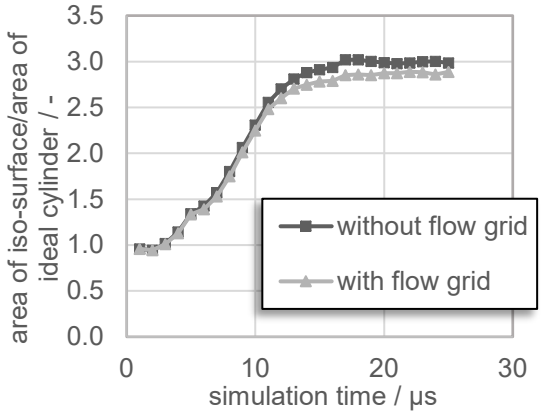

Figure 9. Normalized area of iso-surface (α=0.5) of the waterjet.

Table 4. VOF-LES results

	nozzle with flow grid	nozzle without flow grid
simulation time / µs	21.42	21.42
surface area of iso-surface of water with volume fraction of 0.5 / mm²	26.68	27.55
surface area of cylinder with diameter of the nozzle and the length of the domain / mm²	9.24	

From Figure 9 it can be seen that the waterjet is more coherent with the flow grid. We examined the surface of the waterjet and compared both variations. The iso-surface of the waterjet was related to a cylinder with the diameter of the nozzle and the same length as the waterjet. The iso-surface of the waterjet with the flow grid has a smaller area than the waterjet without the flow grid. The difference is around 3.3 %, which is small, but noticeable. This difference may grow larger if the size of the domain is increased. The smaller surface of the waterjet indicates a more coherent waterjet. The waterjet without the flow grid shows both, a larger wave formation and more ligaments and droplets, Figure 11. Both waterjets show the typical wave formation, as also shown in [11]. This wave instability grows immediately after the nozzle outlet that eventually leads to the formation of ligaments, which are the precursors of drops. Due to surface forces, a ligament is constricted and a droplet can detach. Thus, the simulation reproduced the primary atomization qualitatively well. Upon closer examination, small droplets are noticed which have a high flow velocity. This may be related to the fact that when droplets are only a few grid cells in size, their physical interaction with the ambient air cannot be calculated correctly.

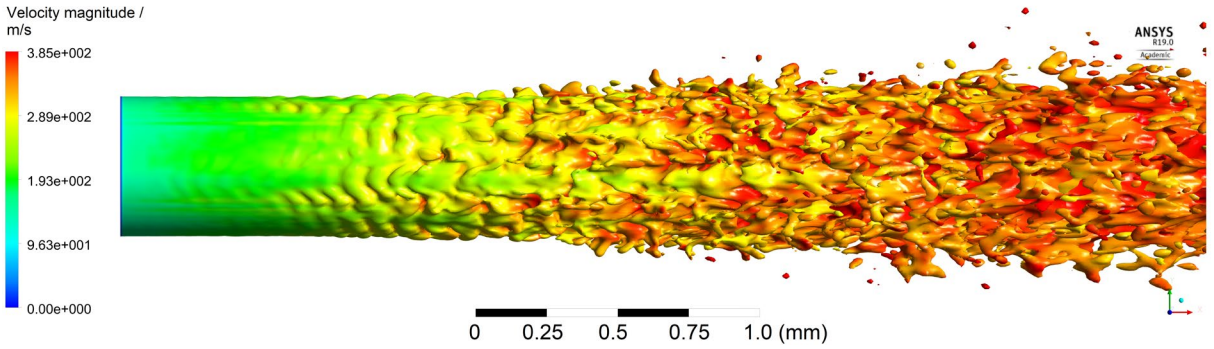

Figure 10. LES-VOF simulation, waterjet *with* flow grid installation (iso-surface of water volume fraction 0.5).

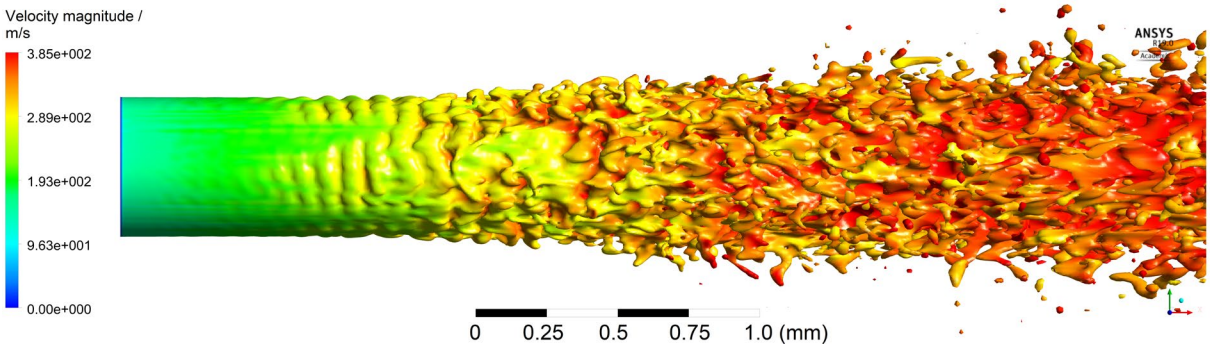

Figure 11. LES-VOF simulation, waterjet *without* flow grid installation (iso-surface of water volume fraction 0.5).

High-speed photography

For the experimental setup, both the original nozzle with the flow grid and a modified nozzle without the flow grid were used. The pressure was set up to 75 MPa, the same value as in the simulation. The nozzle outlet from which the waterjet exits was not visible because the nozzle holder hides it. From the outlet of the nozzle, up until the waterjet can be seen, there is 9 mm distance. Therefore, the first breakup of the waterjet cannot be seen. The high-speed photo in Figure 12 shows a waterjet with the flow grid. When compared to nozzle without the flow grid, in Figure 13, it is noticeable that the nozzle with the flow grid creates a more coherent jet. The jet disintegration takes place, further downstream for the nozzle with the flow grid. Furthermore, the spray angle is lower for the nozzle with the flow grid. A low spray angle is required to maximize the specific energy per unit area on the surface of a component.

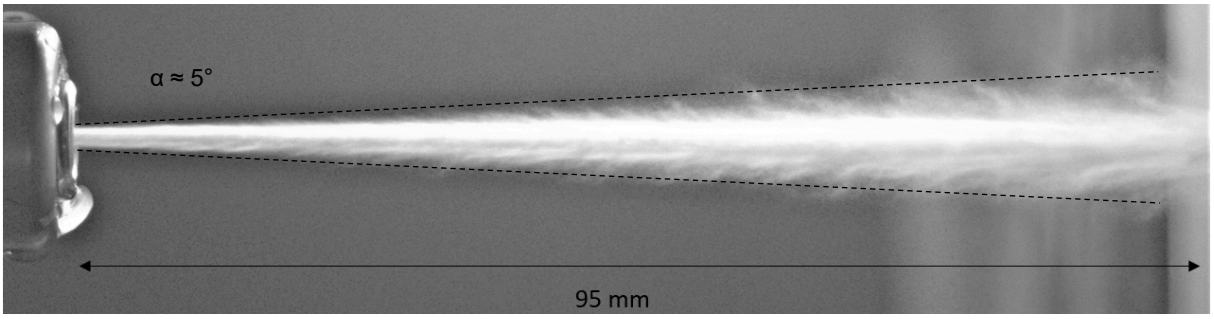

Figure 12. High-speed photograph of waterjet from nozzle with flow grid (~125 ns, with NANOLITE fx xenon flash).

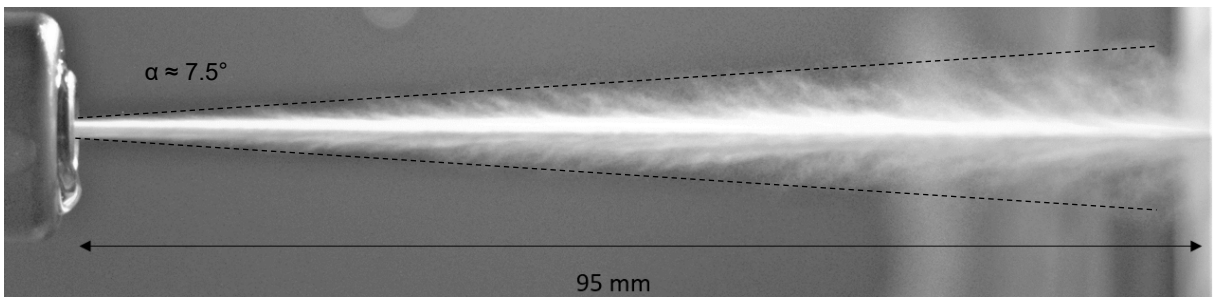

Figure 13. High-speed photograph of waterjet from nozzle without flow grid (~125 ns, with NANOLITE fx xenon flash).

Summary

In this study, the flow inside a HPWJ nozzle at 75 MPa was investigated. The waterjet velocity reaches around 385 meters per second according to our simulations, which matches with the theoretical calculation. With a high-speed photography the dynamics of the waterjet were captured, which revealed a waterjet core surrounded by small droplets. The breakup of the waterjet takes place shortly after exiting the nozzle, as expected. Investigating the waterjet in more detail, the simulations showed the typical behaviour of wave instabilities on the surface of the jet. The instabilities grow, which finally leads to the ligament and droplet development. The effect of a flow grid was studied which had a beneficial effect on the stability of the liquid core in both the simulation and in the experiment. From the photos, the stabilizing effect of the flow grid was proven. The spray angle was significantly lower for the nozzle with the flow grid than for the nozzle without the flow grid. The simulation revealed that the nozzle with the flow grid produces higher levels of turbulence, which seems to be responsible for the higher stability. The approach in this study combined steady state RANS simulation results with computationally higher demanding unsteady LES-VOF simulations.

Conclusion and outlook

According to the subdivision of the flow regime as in [3], the operating conditions of the studied HPWJ-nozzle are in the atomization regime. A liquid core, therefore, should disintegrate shortly after the nozzle outlet. This was however not the case with the studied HPWJ nozzle, which indicates the presence of additional influences, which have a positive effect on the disintegration length. Turbulence produced by a flow grid might be responsible for the stabilization. Therefore, the next step is to investigate other shapes of the flow grid. The stabilizing effect could be significantly increased. It is also planned to run a LES-VOF simulation with the convergent part of the nozzle and the corresponding boundary conditions. Moreover, it is planned to study the effect of the turbulence kinetic energy inside the liquid core more thoroughly. It seems plausible, that higher turbulence inside the liquid core acts as an additional turbulence viscosity, which stabilizes the jet further downstream. This phenomenon will also be studied at higher inlet pressures. Although computationally very demanding the LES-VOF approach shows promising results. The study of high-pressure liquid jets remains a difficult area of research, but it is worth to continue analyzing the effects in order to understand the influences on the atomization process.

Acknowledgements

This work was funded by the German Research Foundation (DFG) under the project: “Experimentelle und numerische Untersuchung des Strömungsprozesses von Hochdruckwasserstrahlen und ihrer Interaktion mit Bauteiloberflächen“, which the authors gratefully acknowledge.

Nomenclature

α	water volume fraction [-]
ρ	density [kg m^{-3}]
ρ_0	reference density [kg m^{-3}]
p	pressure [Pa]
p_0	reference pressure [Pa]
K_0	bulk modulus [Pa]
v_j	jet velocity [m s^{-1}]
v_{th}	theoretical jet velocity [m s^{-1}]
n	density exponent [-]
$\dot{q}$	volume flow rate [m^3 s^{-1}]
c_d	nozzle discharge coefficient [-]
A_0	reference area [m^2]
tke	turbulence kinetic energy [J/kg]

References

[1] M. Hashish, “Visualization of the abrasive-waterjet cutting process,” *Experimental Mechanics*, vol. 28, no. 2, pp. 159–169, 1988.

[2] Frenzel L., “WHAT EFFECT DOES WATERJET CLEANING HAVE ON THE SURFACE AND SURFACE PREPARATION?,” *2007 American WJTA Conference and Expo August 19-21, 2007 Houston, Texas*.

[3] Wolfgang von Ohnesorge, “Die Bildung von Tropfen an Düsen und die Auflösung flüssiger Strahlen: Vorträge der Hauptversammlung in Dresden,” *Zeitschrift für angewandte Mathematik und Mechanik*, no. Band 16, Heft 6, pp. 355–358, 1936.

[4] A. Begenir, H. Vahedi Tafreshi, and B. Pourdeyhimi, “Effect of Nozzle Geometry on Hydroentangling Water Jets: Experimental Observations,” *Textile Research Journal*, no. 74(2), pp. 178–184.

[5] R. D. Reitz and F. V. Bracco, “Mechanisms of breakup of round liquid jets,” *Encyclopedia of Fluid Mechanics*, pp. 233–249, 1986.

[6] T. Susuzlu, A. M. Hoogstrate, and B. Karpuschewski, “Initial research on the ultra-high pressure waterjet up to 700MPa,” *Journal of Materials Processing Technology*, vol. 149, no. 1-3, pp. 30–36, 2004.

[7] *7.3.4. Compressible Liquid Density Method.* [Online] Available: https://ansyshelp.ansys.com/account/secured?returnurl=/Views/Secured/corp/v190/flu_ug/flu_ug_props_comp_liq_den_treat.html. Accessed on: Mar. 05 2019.

[8] F. R. Menter, “Two-equation eddy-viscosity turbulence models for engineering applications,” *AIAA Journal*, vol. 32, no. 8, pp. 1598–1605, 1994.

[9] J. H. Ferziger and M. Perić, *Computational Methods for Fluid Dynamics*. Berlin, Heidelberg, s.l.: Springer Berlin Heidelberg, 2002.

[10] A. Smirnov, S.Shi, I. Celik, “Random Flow Generation Technique for Large Eddy Simulations and Particle-Dynamics Modeling,” *Journal of Fluids Engineering*, no. 123, pp. 359–371, 2001.

[11] J. W. Hoyt and J. J. Taylor, “Waves on water jets,” *J. Fluid Mech.*, vol. 83, no. 01, p. 119, 1977.